Aerodynamic pressures around high-speed trains: the transition from unconfined to enclosed spaces

Baker, C.; Gilbert, T.; Quinn, A.

DOI:
10.1177/0954409713494947

Aerodynamic pressures around high-speed trains: the transition from unconfined to enclosed spaces.

Timothy Gilbert*, Christopher Baker and Andrew Quinn

Birmingham Centre for Railway Research and Education, School of Civil Engineering, University of Birmingham

* Corresponding author: School of Civil Engineering, The University of Birmingham, Edgbaston, Birmingham, West Midlands, B15 2TT, UK. Email: tkg614@bham.ac.uk. Tel: +447563791094.

Keywords: Train aerodynamics, aerodynamic pressures, open air, walls, partially enclosed spaces, tunnels.

Abstract

The theory and practice of train-induced aerodynamic pressure loads on surfaces near to the tracks is compromised by an incomplete understanding of trains operating in short tunnels, partially-enclosed spaces, and next to simple structures such as vertical walls. Unique pressure loading patterns occur in each case. This work has been carried out to obtain a fundamental understanding of how these loading patterns transition from one to the other as the infrastructure becomes more confined. It also considers the impact of the results on two separate European codes of practice applying to tunnels and other structures. A parametric moving-model study was undertaken, transitioning from the open air to single and double vertical walls, partially-enclosed spaces, short single-track tunnels and a longer tunnel. The train model was based on a German ICE2, and was fired at 32m/s past the structures. Multiple surface pressure tappings and in-flow probes were used, providing the opportunity to assess three-dimensionality of the pressure and velocity fields. The experiments successfully mapped the transition between the three loading patterns and isolated the geometric changes. Further loading patterns were discovered relating to the length of the train, the length of the tunnel and the distance from the tunnel entrance. The three-dimensionality of the pressure was related to the length of the tunnel and the distance from the tunnel entrance. Issues surrounding the lack of provision in codes of practice for short tunnels were discussed.

Introduction

High-speed trains generate transient static pressure changes which impose cyclic loads on surfaces close to the tracks. In the open air, the form of the 'loading pattern' is shown in Figure 1 (© British Standards Institution (BSI - www.bsigroup.com). Extract reproduced with permission. Source: BS EN 14067-4:2005+A1:2009 Railway applications. Aerodynamics. Requirements and test procedures for aerodynamics on open track. All rights reserved). The passage of the train nose is marked by a positive peak followed by a negative (suction) peak. The passage of the train tail is marked by a suction peak followed by a positive peak. In codes of practice, the highest loads are assumed to occur around the nose, so nose loads form the basis for assessing pressure loading amplitudes on trackside and overhead structures. European codes include EN 1991-2:2003 [1] and a railway-specific standard EN 14067-4 [2]. These codes were developed from experimental and theoretical work carried out for ERRI [3]. EN 14067-4 includes methodologies for experimental or numerical assessment of loads, and shortcut predictive equations for assessing loads on a limited range of structures. Assessments may be conducted at full-scale or reduced-scale, or numerical simulations may be used. The predictive equations may be applied to vertical walls, horizontal surfaces, mixed surfaces including inclined sections, and tunnels shorter than 20m (formed by vertical walls and a horizontal surface). The predictive equations for vertical walls only apply to walls on one side of the tracks, so this paper includes commentary on the effect of adding walls on the opposite side of the tracks. The equations also assume that the load is linear along the wall's height. This paper comments on how the loads on vertical walls vary with height. The predictive equation for a short tunnel defines the tunnel as a 'closed structure enveloping the tracks', and amplification factors are simply applied to the equations for vertical walls and horizontal surfaces above the tracks, which are based on the assumed loading pattern (Figure 1). This

paper questions whether the loading pattern in Figure 1 is an acceptable assumption for a short tunnel of 20m length, and explores how the loading pattern varies as the tunnel length increases.

Any tunnel longer than 20m is considered in the code of practice EN 14067-5 [4]. As a train enters a tunnel, the air ahead of the train nose is compressed. A compression (positive pressure) wave-front propagates through the tunnel at approximately the speed of sound, whilst gradually dissipating energy. Upon reaching the exit, part of the wave-front energy is reflected as an expansion (suction pressure) wave-front propagating towards the entrance, whilst the rest is emitted out from the exit portal. The reflections continue periodically, whilst frictional losses and portal emissions cause them to decay. As the train nose leaves the tunnel, another compression wave is generated, and as the tail enters and leaves the tunnel, expansion waves are generated. The overall 'pressure wave' pattern is complex. Figure 2 shows an example of a wave pattern measured by a trackside probe, for a tunnel significantly longer than the train's length (). The wave pattern superposes onto the pressure field around the train at locations along the tunnel which are specific to a particular train speed and tunnel length. As the tunnel length decreases, the wave pattern seen by a stationary observer tends towards a sinusoidal shape superposed onto a pressure transient around the train, as was found in experiments reported in Schultz (1990) [6]. This paper examines whether the loading pattern for a 20m long single-track tunnel is more similar to that in Figure 1 or Figure 2, in other words exploring why this length represents the interface between the two aforementioned codes of practice. This paper also examines how the loading pattern is influenced by changing the tunnel length, and the longitudinal positioning of instruments, separately.

EN 14067-5 sets out methodologies for assessing the 'train-tunnel-pressure signature' using trackside instrumentation, in order to assess the conformance of the worst-case total pressure change to criteria for medical health. Full-scale tests, numerical simulations or reduced-scale tests may be used. The minimum tunnel length for carrying out the tests is theoretically 250m (full-scale length). Additional adjustments account for the length and speed of the train, so the 'pressure signature' (loading pattern) is of the required form; That is, the tail-entry expansion wave occurs before the train nose passes the instrument, and the first reflected expansion wave occurs after the train nose passage. Finding the maximum pressure in short tunnels is an issue which is yet to be addressed. This paper explores how the guidance could be changed in order to make the methodology more generally applicable. This paper also questions the code's implicit assumptions that the shape of the loading pattern is identical at any point within the tunnel - it is known that the pressure waves are highly three-dimensional as they are first formed, and may remain highly three-dimensional in short tunnels.

Neither of the aforementioned codes of practice extends to partially-enclosed spaces, which are formed by longitudinal openings in what would otherwise be tunnels. Moving-model tests undertaken by Takei et al. [7] for RTRI found that the form of the loading pattern around the train in a partially-enclosed space is unique, and not like either of the standard patterns in Figures 1 or 2. A positive load occurs around the train nose, and a suction load occurs around the tail. Only one opening width was used in the study, so this observation could not be linked with the standard patterns. Part of this paper considers how the loading pattern evolves between the two main forms when a parameter is introduced, which describes a gap in a tunnel cross-section that permits leakage. This paper will attempt to relate results from this study with those from the RTRI study.

In order to explore all of the aforementioned issues, a parametric experimental study was undertaken, for the lead author's PhD thesis, at the 'TRAIN Rig' moving-model facility in Derby (UK), which is owned and operated by the University of Birmingham. This paper aims to explore the transition from unconfined to confined spaces, by working from the open air, to single and double vertical walls (in symmetrical and asymmetrical configurations), partially-enclosed spaces, short single-track tunnels, and a longer tunnel. Instruments were placed into the air gap between the train and wall, and lines of pressure tappings were drilled into the structures, in the longitudinal, lateral and vertical directions. Therefore, the loading pattern and temporal evolution of the pressure transients has been studied in three-dimensions. This paper compares the pressure transients very close to structure surfaces with surface tapping measurements, and also with measurements very close to the train side. Therefore, a second aim of this paper is to provide useful insights into the effect of instrument type and placement.

The details of the experiments and data analysis techniques are explained in the section 'Methodology'. Some results are compared against the results of other investigations in the section 'Validation'. The results are presented and discussed in three sections: 'Open air and walls'; 'Short tunnels'; and 'Partially-enclosed spaces'. The conclusions and recommendations for further work are described in the final section.

Methodology

TRAIN Rig and experimental model

Tests were undertaken at the 'TRAIN Rig' moving-model facility. It consists of a 150m long track along which reduced-scale model vehicles can be propelled at speeds of up to 75m/s. It is one of few aerodynamic facilities which are able to account for relative movement between vehicles, the ground, and complex structures such as train stations and tunnels. A 1/25 scale model 'simplified ICE2' train was built, based on the aerodynamic shape of a German ICE2; it is shown in Figure 3.

A number of simplifications were made. Firstly, the model featured four carriages, which was less than the usual eight or sixteen carriage configurations of the ICE2. Secondly, detailed components such as bogies were geometrically simplified. Thirdly, a flat track profile was used without consideration of a ballast shoulder. Finally, the test speed of 115kph (32m/s) was less than the 280kph operational speed of the ICE2. The corresponding Reynolds number was 305,000 based on the speed and body height of the train (143mm at 1/25 scale). The reduced speed was necessary to meet the requirements imposed by a companion study which analysed the slipstream velocity (Gilbert et al. 2013 [8]). However, a previous study by Johnson and Dalley [9] found that reduced Reynolds numbers did not compromise the accuracy of the results; the pressure transient on the side of a stationary train was measured as it was passed closely by a moving-model train. The study found a linear relationship between the peak pressure on the stationary train, and the square of the speed of the passing train, which was fired at speeds between 33m/s and 52m/s. This relationship suggests a lack of sensitivity to Reynolds number. From this we may presume, that peak pressure measurements on vertical walls can be extrapolated to full scale conditions accurately, if the side of the stationary train

is analogous to a vertical wall. However, in tunnels, the moving-model test speed must be identical to the full-scale operating speed. This is because the magnitude of the train-entry compression wave-front is related to the train speed by a different relationship to that which describes the transient around the train nose itself. Moreover, the superposition pattern between the pressure waves and the train pressure field changes in relation to the tunnel length and train speed. Therefore, the results for tunnels and partially-enclosed spaces should not be extrapolated for analysis outside the context of the discussion in this paper, without consideration of these scaling issues.

The model speed was measured upstream and downstream of the entrance and exit of the structure using pairs of light gates. Each pair was spaced 1m apart, and the speed was calculated based on the time taken for the model to break both beams. The upstream and downstream pairs of light gates were 9m apart, separated longitudinally, and test structures were placed in the intervening space. The model speed was estimated at each probe and tapping position using a linear interpolation of the two speed measurements. The deceleration of the train through the test section was ignored. 99% of the tested speeds were within 5.2% of the target speed of 32m/s.

Geometry and flow variables

Positions in this paper are referred to using dimensionless x/Z, y/Z, and z/Z terms to avoid confusion regarding scale. x, y and z are the longitudinal, lateral and vertical directions relative to the direction of travel, with x originating from the tip of the train nose, y from the track centre, and z from the railhead. X, Y and Z are the dimensions of the train. The full-scale equivalent dimensions are X=105.4m (length), Y=3.075m (width), and Z=3.9m (height). The

1/25-scale dimensions (as built) are X=4.216m, Y=0.123m, and Z=0.156m. The length of a structure is denoted by L, and a dimensionless term L/Z is used. The distance of the instrument from the structure entrance is denoted by x_P, given either as a dimensionless term x_P/Z, or a percentage of tunnel length based on x_P/L. Some useful reference values are defined: The positions of the nose and tail of the train are x/Z=0 and 27 respectively; the distance of the side of the train from the track centre is y/Z=0.39; the height of the top of the train above the top of the rail is z/Z=1; the height of the top of the rail above the flat ground is z/Z=0.077; and the rail heads are approximately y/Z=0.39 apart (1.535m at full-scale). Two geometric dimensionless variables are defined: The blockage ratio β is the cross-sectional area of the train divided by the cross-sectional area of the tunnel; and the leakage ratio α is the width of a gap in the cross-section of a tunnel divided by the cross-sectional internal perimeter of a tunnel.

The static pressure data were converted into a dimensionless coefficient form:

$$C_P = \frac{P}{0.5\rho V^2}$$

The peak-to-peak pressure change is:

$$\Delta C_p = \max C_P - \min C_P$$

P is the measured static pressure, ρ is the ideal gas density of air, and V is the train velocity.

Test cases

Figure 4 shows cross-sectional views and geometric details of the structures used in the tests. The wall cases were divided into single and double configurations. Of the double configurations, two cases were arranged symmetrically about the y-axis, and one case was arranged asymmetrically. The single configurations consisted of three lateral separations from

the track centre. Four lengths of fully sealed tunnels were tested. T1 was considerably longer than the other tunnels, for the purpose of assessing the difference between a long and short tunnel. Tunnels T2-T4 were rectangular in cross-section, and T1 had a circular cross-section, as it was a pre-existing structure at the TRAIN Rig. The rectangular tunnels could not match the cross-sectional area and internal perimeter of T1 exactly. Therefore, the cross-sectional area of T1 was 0.4% higher than the rectangular tunnels, and its internal perimeter was 9% lower. The increased cross-sectional area of T1 alone may cause approximately a 0.5% decrease in the pressure rise across the initial compression wave-front (according to the approximate formulation given in Howe et al. [10]). All tunnels but the shortest (T4) featured vertical-faced portals at their ends. T3 included partially-enclosed variations in which a continuous gap of adjustable size ran along the length of the tunnel ceiling. T2 also included one partially-enclosed variation. T4 was equivalent in length to a 20m tunnel, making it the minimum length to be considered a tunnel in EN 14067-5, and also the maximum length to be considered an 'enclosed structure' in EN 14067-4. The blockage ratio of all the tunnels was β=23%.

Instruments and ensemble analysis

The static pressure was measured using a combination of 'surface tappings' and 'in-flow' probes. The surface pressure was measured using the surface tappings which were flush-mounted on the structure surfaces. The surface tappings were connected to 30mm long silicone tubes, which connected to single-ended pressure transducers from the Sensortechnics HCLA 12X5PB series. Their calibrated frequency response was 2000Hz. The pressure was measured within a range of ±1250Pa relative to a reference atmospheric pressure. The reference pressure was measured at a location away from the flow which was not susceptible to aerodynamic effects from the train. Most cases included a line of five surface tappings along a vertical wall, so the variation of the pressure with z could be assessed. Their exact positions are given in the

results sections. In the short tunnels, three surface tappings were added to the ceiling, so the variation of the pressure with y could be assessed. The results are presumed to be symmetrical about the y-axis, based on the findings in Baker et al. [11], in all cases apart from the asymmetrical wall configuration (W3D) and the single walls (W1S, W2S, W3S). Surface tappings were only installed on the right sides of the structures. For the asymmetrical walls (W3D), this corresponded to the side closest to the train. In the short tunnels, additional surface tappings were installed at various longitudinal positions, so the variation of the pressure on the walls with x_P and L could be assessed.

'TFI' Cobra Probes measured the in-flow pressure. The probes came from two batches; the calibrated frequency response was 650Hz for one batch and 2000Hz for the other. Two near-wall probes were installed at near-identical lateral distances of 0.06Z and 0.09Z from the wall surface, and at respective heights of z/Z=0.05 and 0.58 above the railhead. The lateral distances were not identical due to constraints on probe positions for a separate simultaneous study using the Cobra Probes. One near-train probe was installed at y/Z=0.11 and z/Z=0.58. Additional Cobra probes were used in the open air and wall cases, so data for more positions were available for z/Z=0.58. Individual scans of the pressure data measured by the Cobra Probes were replaced with zeros if the flow angle exceeded the 45 degree 'cone of acceptance'. Zeros were most common around the nose and first carriage. Peak pressure results are not plotted or discussed if zeros affected their values.

All data in this paper were measured at 5000Hz and low-pass filtered using a fifth order zero-phase Butterworth filter with a cutoff of 250Hz. This is equivalent to 10Hz at full-scale. This accounts for the differences in sensitivity between the Cobra probes from the different batches.

The ‘ensemble averaging’ technique was employed in these tests. It is described in Sterling et al. [12]. Although principally used in the study of slipstreams, it may also be used in the assessment of pressure transients. The tests were repeated multiple times to form ensembles. The ensembles were aligned to a common point at the train nose. To account for slight speed variations between runs, the pressure from each run was normalized into its dimensionless coefficient form C_P. The data were re-sampled on the time axis to prevent runs from drifting apart with increasing distance from the nose alignment point. The ensemble formed an array aligned to a common time axis, so the ensemble average was obtained by averaging the data at each time increment.

The uncertainty of the ensemble average was examined using the results from a test case (W1D) in which the signal-to-noise ratio of C_P was low making it somewhat of a worst case. A Monte Carlo simulation, using random combinations of runs, found that the 95% confidence limit of the standard error of the mean of ΔC_P was 1% for 2 runs, decreasing to 0.13% for 25 runs. The ensemble sizes that were achieved in the experiments varied from 2-5 runs for the single walls, to 5-25 runs for all other structures. Although some experiments were only repeated a small number of times, the estimated accuracy was still within ±1%. The large variation in ensemble sizes was due to a combination of changing time constraints, and the requirements of a separate study assessing the flow velocities (Gilbert et al. [8]), which needed larger ensembles to reduce the uncertainty of the turbulent velocity fields to an acceptable level.

Validation

Open air pressure measurements were undertaken recently as part of the AeroTRAIN project (summarized in Sima et al. [13]), using a full-scale ICE2 train travelling in the open air at high speed. In this study, tests were undertaken with in-flow probes placed in two positions matching those of the full scale experiments, equivalent to y=2.5m, and z=1.5m and 3.3m. The differences in the peak-to-peak pressure changes between the full scale and model scale results at the lower and higher positions are 0.8% and 4.2% respectively, with these results showing higher pressures in both cases. We may conclude that this methodology is acceptable. It does not prove that the results in confined spaces are scalable; particularly in short tunnels where correct Mach number scaling is important, requiring testing close to operational train speeds.

Open air and Walls

Effect of lateral and vertical position

Figure 5 compares the loading pattern, measured by an in-flow probe, of the open air with the symmetrical double wall case W2D. The walls increase the peak pressure magnitudes relative to the open air. Figure 6 shows the peak pressures around the train nose, measured by in-flow probes at multiple *y*-axis positions, comparing the open air with the symmetrical double wall cases W1D and W2D. Figure 6(a) shows the peak positive and suction pressure in each case, whilst Figure 6(b) shows the peak-to-peak pressure change. Note, the 'max' and 'min' lines for the walls start from different *y*-values because zeros in the Cobra probe data hid the suction peaks for some time histories. The results show that walls cause the peak pressures to increase, as expected. The positive peaks increase more than the suction peaks.

Figure 7 shows the peak-to-peak pressure around the train nose, this time measured by surface tappings at multiple *z*-axis positions, comparing the open air with all of the wall cases. These cases include three single walls (W1S, W2S, W3S), and three double walls (W1D, W2D, W3D), with one of the double wall cases configured asymmetrically (W3D). The results for all of the walls vary with height. The maximum pressure occurs in the range of 40-60% of the train body height, and a minimum occurs close to the ground and the train roof. Since the top edge of the wall is much higher than the train roof (z/Z=1.79), an 'edge effect' caused by the top of the wall is not deemed responsible for the drop in pressure with height. Rather, this observation is attributed solely to the aerodynamic shape of the train. The mean increase in ΔC_P caused by the symmetrical double walls compared to the single walls is 17% and 16%, for W1 and W2 respectively. The mean increase caused by the asymmetrical double walls W3D compared to the single wall W3S was less, at 12%. This is understandable, because the opposite

wall was further away from the train side than the instrumented wall, rather than the same distance.

Short tunnels

Wave patterns due to compressible flow

Figure 8 shows the pressure field for tunnels of two lengths, measured by surface tappings installed approximately halfway along their lengths. Results for fully sealed (α=0%) and slightly unsealed (α>0%) tunnels are shown. The gaps in the unsealed tunnels may cause the pressure waves to decay rapidly, leaving just the generic loading pattern caused by the train. This generic loading pattern is somewhat like that which is shown in Figure 1, but the compression region is still visible ahead of the train nose, and it is the phenomenon responsible for causing the maximum positive pressure. In the sealed tunnels, the pressure wave reflections decay slowly, causing an oscillation to be superposed onto the generic loading pattern. The results also show that the highest suction peak occurs between the nose and tail of the train. This assumption is generally shared in EN 14067-5. The loading pattern observed for the two lengths are different; this will be explored in the next section.

Effect of tunnel length, longitudinal position and train speed

This section discusses how the tunnel length, the placement of the surface tapping along the *x*-axis (longitudinally), and the train speed together affect the loading pattern. Figure 9 shows how the loading pattern varies based on a surface tapping's *x*-axis position, while the tunnel length and train speed are constant. In Figure 9(a), two positions are shown for T2, and in Figure 9(b), three positions are shown for T3. The results show that as the distance from the entrance increases, the following changes occur: The positive peak pressure magnitude ahead of the nose decreases; the suction peak magnitude just behind the nose increases; the suction peak magnitude just ahead of the tail increases; and the positive peak magnitude behind the tail decreases. The reduction of the maximum positive peak pressure is caused by pressure wave

reflections - expansion waves superpose onto the positive pressure region ahead of the train nose. Figure 9(b) shows that the peak suction pressure magnitude remains similar at all three positions. The results also show that the peak suction pressure between the nose and tail either remains negative along the whole train length, or returns to atmospheric (C_P=0), depending on the tunnel length and probe position. Overall, it may be said that suction pressure region will remain negative along the whole train only if the entire train is within the tunnel. More specifically, it occurs if the tail-entry expansion wave has been detected, whilst the nose-exit compression wave has not.

Figure 10 shows how the loading pattern varies based on the tunnel length, while the surface tapping's *x*-axis position and train speed are constant. These results suggest that the tunnel length greatly affects the peak pressure magnitudes. This behaviour is related to the distance of the tunnel's exit from the measuring point, as this controls the superposition pattern between the pressure field around the train and the pressure waves. The results show that the peak positive pressure is lower in the shorter tunnels, because the first expansion wave (reflected from the tunnel exit) occurs longer before the peak is reached. Also, the near-entrance tappings detect higher peak positive pressures than those installed further from the entrance. An analytical equation can be developed, defining a region in which the tunnel length has no effect on the results. If the first expansion wave reflected from the tunnel exit is detected after the train has passed a point in the tunnel, the tunnel length has no effect on the pressure field around the train at that point. The following equation represents the dimensionless position within the tunnel where the first reflected pressure wave and a user-specified position (x) relative to the train nose are at the same point:

$$\frac{x_P}{L} = \frac{2M - \frac{x}{L}}{M+1}$$

x_P/L is the dimensionless position within the tunnel, and M is the Mach number of the train (assuming the mean wave propagation speed is equal to the speed of sound). The following condition must be met:

$$0 \leq x_P \leq L$$

The equation assumes that the time taken for the nose-entry compression wave to travel from the tunnel entrance to the exit at the speed of sound, then for the first reflected expansion wave to travel from the exit to back to x_P, is the same as the time taken for the selected point on the train to travel from the tunnel entrance to x_P+x at speed V. The equation represents the boundary between two regions:

1. When LHS>RHS, a change in tunnel length affects the loading pattern.
2. When LHS<RHS, a change in tunnel length does not affect the loading pattern.

As $L\rightarrow\infty$, or $x\rightarrow 0$, the x/L term may be neglected, so the equation reduces to a generic form in which the tunnel length does not need to be known initially. Figure 11 shows the boundary between the two regions. It is clear that even with these extremes, Region 1 fills the majority of the tunnel, even for the fastest train speeds. An example for T1 is also shown in Figure 11, with $x=X$, highlighting that in these experiments, for the test speed used, it was impossible for the tail of the train to be inside the tunnel before the reflected pressure waves filled the tunnel - the Mach number would need to have been much higher.

To assess conformance to the medical health criterion in EN 14067-5 using full-scale tests, the measured 'train-tunnel-pressure signature' must consist of a series of pressure changes occurring in a prescribed order. These are the nose-entry compression wave, followed by the tail-entry expansion wave; followed, finally, by the passage of the train nose past the observer. The first reflected expansion wave does not form part of this signature. Therefore the equations

in the code for determining the minimum tunnel length and instrument position are designed to ensure a Region 2 pressure signature, which is independent of tunnel length.

It impossible to assess short tunnels, such as those tested in this study, in accordance with the guidance in EN 14067-5. For an eight carriage ICE2 travelling at its operating speed of 280kph, a tunnel length of 1140m is required to accommodate a probe in Region 2. Given that the pressure at a given position in Region 2 is independent of tunnel length, a different approach may be possible. For example, if the requirement that the tail-entry expansion wave occurs before the train nose passes the probe is relaxed, so they may occur in the reverse order, a shorter tunnel may be used, whilst maintaining Region 2 results. With x=0, this equation may be used as a starting point for determining probe positions in such a case.

A final observation relating to tunnel length is that of the minimum threshold for a tunnel, which is currently 20m (the length of T4). The results for T4, shown in Figure 10(c), show a loading pattern more similar to Figure 1 than Figure 2, as pressure wave reflections are not visible in the time history. The use of amplification factors in the predictive equations in EN 14067-4 may therefore be justified for T4, but not necessarily for longer tunnels where pressure wave reflections superpose onto the peaks. However, the assumption in this code that the positive and suction loads occur over 5m (x/Z=1.28) lengths around the train nose is not appropriate to this case; the positive pressure load occurs over a greater length, due to a contribution from a nose-entry compression wave.

Effect of lateral and vertical position

Figure 12 shows the variation of the surface and in-flow peak-to-peak pressures in the tunnel cross-section. Along the vertical walls, the peak-to-peak pressure change is higher than the walls and open air. The results are not linear, and the pattern of variation between the highest and lowest peak-to-peak pressures on the tappings is not substantially different to that seen in the wall test cases (see Figure 7). Further analysis reveals that the positive pressure peaks are more linear than the suction pressure peaks, particularly for the longer tunnels. This is because the positive peaks are caused by the nose-entry compression wave, which becomes near-one-dimensional a short distance from the tunnel entrance. The suction peaks occur between the first carriage and tail of the train, which is a region of greater three-dimensionality. The results also show that for T3 and T4, ΔC_P increases as y decreases, as was found previously in moving-model tests on 'overbridges', presented in Baker et al. [11]. Moreover, ΔC_P increases as z increases, which contrasts with the findings for the walls. The opposite is true for T2 - ΔC_P increases as y increases and z decreases. However, the differences are very small in relation to the overall magnitudes, and the results are quite close to one-dimensional. For T3 and T4, the near-wall in-flow pressure changes are very dissimilar to the surface pressures, despite being measured very short distances from the surfaces. Moreover, for T2, the near-wall pressure change is higher than the near-train pressure change. The opposite behaviour would normally be expected, as the pressure field around the train normally decays with growing distance from the train's side. These results suggest that the peak-to-peak pressure change in the shorter tunnels (T3 and T4) is highly three-dimensional. The accuracy of one-dimensional tunnel analysis simulations may be compromised for short tunnels, and experimental results are highly sensitive to probe placement.

Partially-enclosed spaces

Effect of leakage ratio and longitudinal position

Figure 13 shows time histories near the entrance, middle, and exit of T3 for two values of leakage ratio (α). The results for α=0% are included, as well as case W1D (in which the gap between the walls is equivalent to α=24%), to represent two extremes. A clear transition occurs between the two main loading patterns of Figure 1 and Figure 2. There are hints that the loading pattern previously found in Takei et al. [7] has been observed (a single positive pressure peak around the nose and a single suction peak around the tail) - for example, see Figure 13(b) for α=4.3%. The results also show that the reflected pressure waves are fully damped at α=0.4%. Peak pressure magnitudes generally reduce with increasing α. The form of the loading pattern changes most significantly from α=0.4% to 4.3%.

Closer inspection of the pressure time histories of the ceiling surface tappings (not plotted) suggests that compressed air ahead of the train nose flows out of the gap, and re-enters just ahead of the train tail when a suction pressure occurs inside the tunnel. The variation of the results between the entrance, middle and exit shows that tunnel length still has some effect on the observations, even at α=4.3%. A longer partially-enclosed tunnel was tested, and its results can be seen in Figure 8(a).

Effect of lateral and vertical position

Figure 14 shows the variation of surface and in-flow peak-to-peak pressures in the cross-section, for four α values. The results for the extreme cases of α=0% (T2) and α=24% (W1D) are plotted in Figures 12 and 7 respectively, and will be taken into account. These results show that the peak-to-peak pressure magnitudes are higher than the walls and open air, but lower

than in the short tunnels. The results are not linear, and the variation between the highest and lowest peak-to-peak pressures on the tappings is not substantially different to that seen in T2 or W1D. Further analysis has found that, as with the tunnels, the positive peak is more linear than the suction peak, particularly for the lower α values. For the three lower α values, ΔC_P increases with increasing z, and decreasing y. The same pattern was found for the enclosed tunnels (Figure 12). For α=1.4% and 4.3%, there is a bulge in the range of 60-80% of the train's body height. A similar pattern occurs for the walls (W1D, Figure 7). There is also an increase in pressure with increasing z, which occurs in tunnels. Therefore, it may be said that as α increases, the pattern of pressure variation around the cross-section transitions from tunnel- to wall-type behaviour, starting from around α=1.4%. The in-flow and surface pressure measurements correspond more closely than in the short tunnels (in the one case where in-flow probes were used, α=4.3%). Further analysis of the ceiling tapping pressures found that the suction pressure magnitude is higher on the ceiling than the walls. For the surface tappings closest to the opening, the suction peak pressure is higher in magnitude than the positive peak - this was not seen in the other results of these experiments, and it may be due to a pressure gradient around the adjacent gap.

Conclusions and further work

Moving-model experiments were conducted to measure the transient aerodynamic pressure around a simplified ICE2 train operating in confined spaces, starting from the open air, then transitioning to single and double vertical walls, partially-enclosed spaces, short tunnels and a longer tunnel. From this work the following conclusions may be drawn:

1. The pressure on a wall surface increases when another wall is placed on the opposite side of the tracks.
2. Different aerodynamic pressure loading patterns occur in the tunnel, partially-enclosed space, and wall test cases. The patterns have been linked by varying the size of an opening in a tunnel ceiling.
3. In most positions within tunnels, the maximum positive pressure is attenuated by the superposition of reflected expansion waves from the tunnel exit. An analytical equation has been used to show the range of tunnel positions in which the observed peak pressures are not affected by tunnel length.
4. The assumption that maximum pressure loads occur directly around the nose of the train is only valid for the open air, walls, and a tunnel with a length equivalent to 20m at full-scale. In the other cases, different loading patterns have been observed either due to pressure waves or the presence of openings in the structures.
5. Distinct pressure loading patterns occur in tunnels when the train nose and tail are not simultaneously inside the tunnel.
6. Codes of practice are biased towards longer tunnels when used to determine siting requirements for assessing pressure changes. A modification allowing the train nose to reach the probe before a tail-entry pressure wave, would allow shorter tunnels to be assessed whilst allowing all of the required pressure changes to be measured.

7. The pressure field is highly three-dimensional close to the tunnel entrance and in very short tunnels. Near-wall in-flow pressures in the air gap between the train and the tunnel qualitatively correlate with surface pressure measurements on vertical walls, but not in partially or fully enclosed short tunnels where significant differences have been observed.

Further work should test these conclusions using trains with different aerodynamic shapes, including more modern and streamlined rolling stock, and aerodynamically rough trains. More tests are needed to verify whether the conclusions are valid when variables are changed beyond the ranges used in this study. Variables that were fixed in this study should be changed, including the height of the walls, the length of the partially-enclosed spaces, the positioning of the opening in the partially-enclosed spaces, and the blockage ratio. The validity of α as a parameter for determining leakage effects should be verified with further experiments.

Acknowledgements

The authors would like to thank Deutsche Bahn for providing data on open air pressure pulses for the validation study. The authors are indebted to Dr. Sarah Jordan, David Soper and Martin Gallagher from the University of Birmingham, for their help with performing the moving-model experiments.

Funding

The first author was supported by a studentship from the Birmingham Centre for Railway Research and Education during the course of the doctoral study.

References

1. BS EN 1991-2:2003. BSI Eurocode 1: Actions on structures - Part 2: Traffic loads on bridges.

2. BS EN 14067-4:2005 +A1:2009. Railway applications - Aerodynamics - Part 4: Requirements and test procedures for aerodynamics on open track.

3. ERRI D189/RP1, 1994. Loading due to dynamic pressure and suction from railway traffic. Effect of the slipstream of passing trains on structures adjacent to the track.

4. BS EN 14067-5:2006 +A1:2010. Railway applications - Aerodynamics - Part 5: Requirements and test procedures for aerodynamics in tunnels.

5. BS EN 14067-3:2003. Railway applications - Aerodynamics - Part 3: Aerodynamics in tunnels.

6. Schultz M. Experimentelle und rechnerische Ermittlung von Druckwellenausbreitungsvorgängen bei der Fahrt eines Zuges durch einen kurzen Tunnel. Unterschung des Einflusses der instationären Wandreibung auf die Wellendämpfung. PhD Thesis, Technischen Universität Wien, Austria, 1990.

7. Takei Y, Izumi Y, Yamada S, Iida M and Kikuchi K. Evaluation method for air pressure variation and station facility member deterioration caused by high-speed train passage in stations. *QR of RTRI* 2008; 49(2): 89-95.

8. Gilbert T, Baker C and Quinn A. Gusts caused by high-speed trains in confined spaces and tunnels. Submitted for publication to Journal of Wind Engineering and Industrial Aerodynamics 2013.

9. Johnson T and Dalley S. 1/25th scale moving model tests for the TRANSAERO project. In: Schulte-Werning (ed) *TRANSAERO- A European initiative on transient aerodynamics for railway system optimisation.* Berlin, Germany: Springer-Verlag, 2002, pp.123-135.

10. Howe M, Iida M, Fukuda T and Maeda T. Theoretical and experimental investigation of the compression wave generated by a train entering a tunnel with a flared portal. *Journal of Fluid Mechanics*; 425: 111-132.

11. Baker C, Jordan S, Gilbert T, Quinn A, Sterling M, Johnson T and Lane J. Transient aerodynamic pressures and forces on trackside and overhead structures due to passing trains. Part 1 model scale experiments Part 2 standards applications. *Proceedings of the Institution of Mechanical Engineers Part F: Journal of Rail and Rapid Transit*. Epub ahead of print 27 November 2012. DOI: 10.1177/0954409712464859.

12. Sterling M, Baker CJ, Jordan SC and Johnson T. A study of the slipstreams of high-speed passenger trains and freight trains. *Proceedings of the Institution of Mechanical Engineers Part F: Journal of Rail and Rapid Transit* 2008; 222(2): 177-193.

13. Sima M, Grappein E, Weise M, Paradot N, Heike M, Baker C, Licciardello, R and Couturier M. Presentation of the EU FP7 AeroTRAIN project and first results. In: *9th world congress on railway research,* Lille, France, 22-26 May 2011.

Appendix 1

Notation

α	Leakage ratio (ratio of gap width to cross sectional perimeter of tunnel)
β	Blockage ratio (ratio of cross sectional area of train to area of tunnel)
C_P	Pressure coefficient $P/0.5\rho V^2$
ΔC_P	Peak-to-peak pressure coefficient
L	Length of the structure (m)
M	Mach number (train speed divided by speed of sound, 330m/s)
V	Train speed (m/s)
P	Measured pressure (Pa)
ρ	Density of air (kg/m^3)
x	Distance from the train nose (m)
X	Length of the train (m)
x_P	Position of instrument in tunnel (m)
y	Lateral distance from the track centre (m)
Y	Maximum width of the train (m)
z	Vertical distance above the top of the rail (m)
Z	Maximum height of the train above the top of the rail (m)

Figure 1. Typical transient pressure time history caused by a passing train, from EN 14067-4 [2] ©.

Figure 2. Typical transient pressure time history caused by a passing train in a tunnel. A wave diagram is used to indicate the propagation of compressible flows through the tunnel, from EN 14067-3 [5] ©.

Figure 3. Photograph of the ICE-2-shaped train model.

Figure 4. Cross-section views and descriptions of the structures.

Figure 5. Time history of the pressure field around the train, in the open air and symmetrical double wall case W2D. An in-flow probe was located at x_P/Z=31, y/Z=0.65, z/Z=0.58.

Figure 6. Open air and double wall cases. Variation of in-flow pressure along the y-axis, at height z/Z=0.58. (a) Maximum and minimum pressure; (b) Peak-to-peak pressure change.

Figure 7. Wall cases. Variation of the peak-to-peak surface pressure change along the z-axis, for single and double wall cases.

Figure 8. Short tunnels. The effect of pressure waves; The pressure in a sealed tunnel, measured by a surface tapping, is compared with the pressure in an unsealed tunnel which allows the pressure waves to dissipate quickly. The tapping location is z/Z=0.26. Tunnels: (a) T2, where L/Z=51 and x_P/L=62%; (b) T3, where L/Z=13 and x_P/L=45%.

Figure 9. Short tunnels. The pressure measured at various locations within the tunnels, expressed as dimensionless percentages (x_P/L). The surface tapping height is z/Z=0.26. The tunnels are sealed (α=0%). Vertical lines represent the train nose entering the tunnel. Tunnels: (a) T2, where L/Z=51; (b) T3, where L/Z=13.

Figure 10. Short tunnels. The pressure measured for tunnels of different lengths, when the surface tapping is at a constant distance from the entrance. The tunnels are sealed (α=0%). The tapping height is z/Z=0.26, and the distance of the tapping from entrance in each plot is: (a) x_P/Z=31; (b) x_P/Z=6; (c) x_P/Z=2.6.

Figure 11. Tunnels. Visualization showing how far into a tunnel an observer may detect the same results at a given point relative to the train nose (x) regardless of tunnel length (L). Two values of x and L are plotted.

Figure 12. Short tunnels. Variation of the peak to peak pressure change for the wall and ceiling tappings, and in-flow probes, for tunnels: (a) T2, where L/Z=51 and x_P/L=62%; (b) T3, where L/Z=13 and x_P/L=45%; (c) T4, where L/Z=5 and x_P/L=50%.

Figure 13. Partially-enclosed spaces (L/Z=13). Pressure measured for four α values at three x-positions within the structures. The tapping height is z/Z=0.26. Locations: (a) x_P/L=20%; (b) x_P/L=45%; (c) x_P/L=80%.

Figure 14. Partially-enclosed spaces (L/Z=13). Variation of the peak to peak pressure change for the wall and ceiling tappings, and in-flow probes, for α values: (a) α=0.2%; (b) α=0.4%; (c) α=1.4%; (d) α=4.3%.

Figures

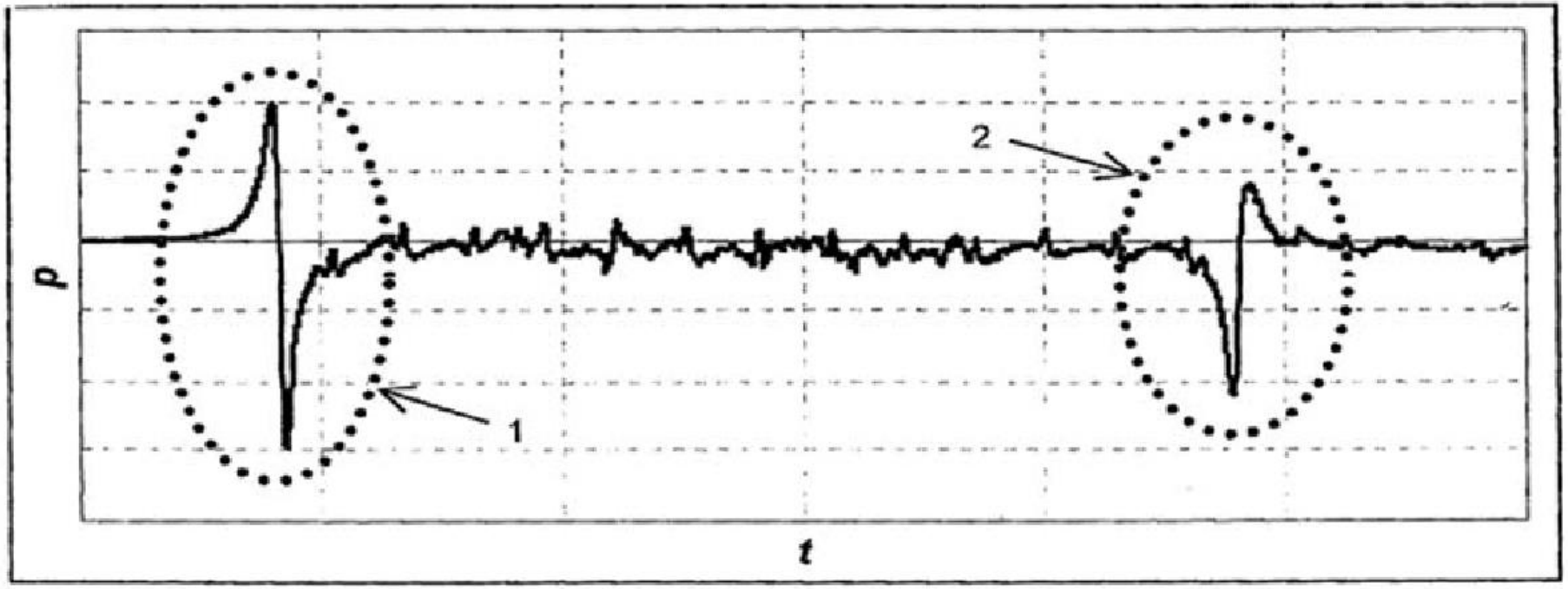

Key

1 Head of train passing

2 Tail of train passing

Figure 1. Typical transient pressure time history caused by a passing train, from EN 14067-4 [2].

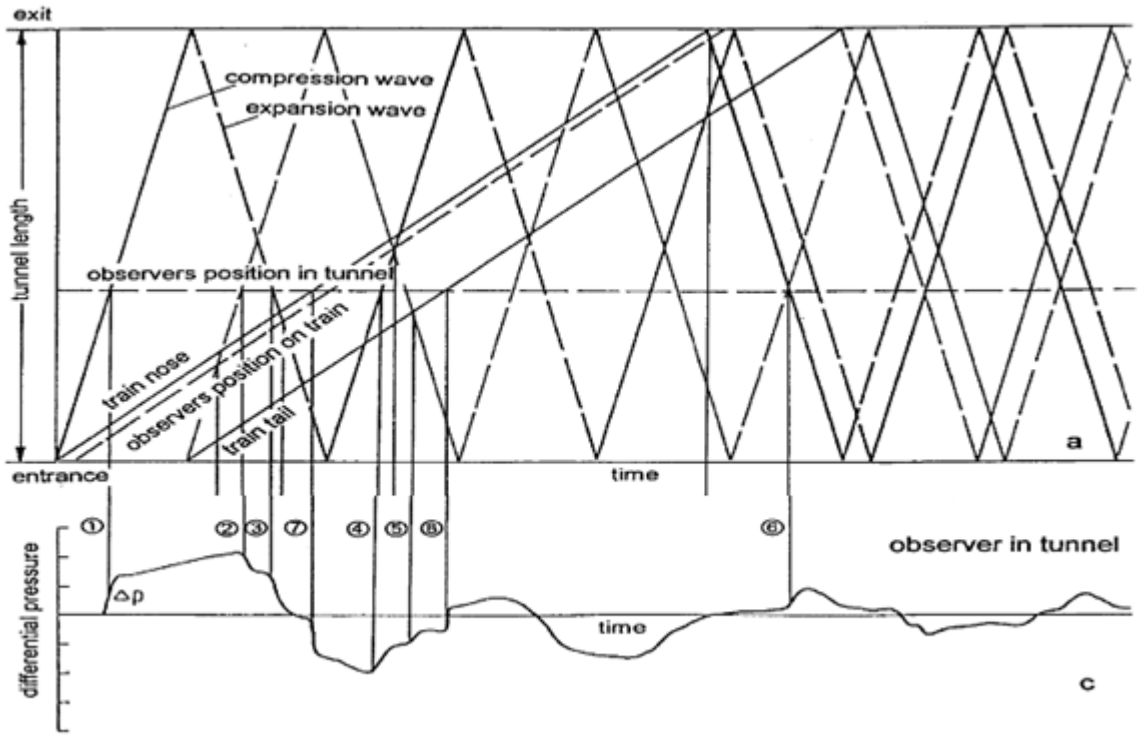

Figure 2. Typical transient pressure time history caused by a passing train in a tunnel. A wave diagram is used to indicate the propagation of compressible flows through the tunnel, from EN 14067-3 [5].

Figure 3. Photograph of the ICE-2-shaped train model.

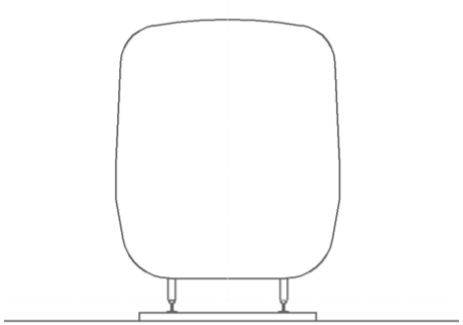

OA. Open air reference data.

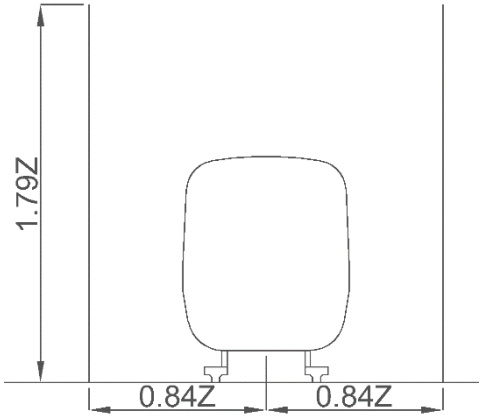

W1S. *L/Z*=51. Right wall only.

W1D. *L/Z*=51. Double walls. Symmetrical.

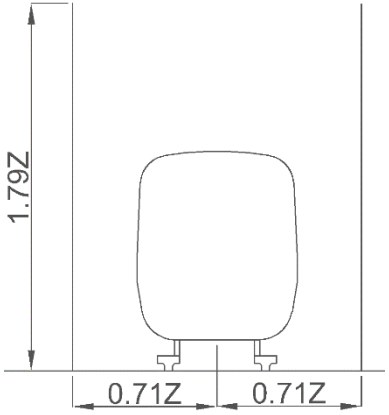

W2S. *L/Z*=51. Right wall only.

W2D. *L/Z*=51. Double walls. Symmetrical.

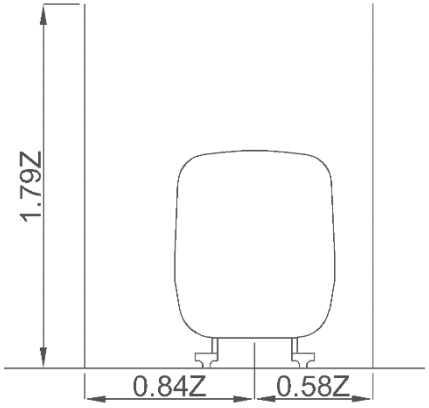

W3S. *L/Z*=51. Right wall only.

W3D. *L/Z*=51. Double walls. Asymmetrical.

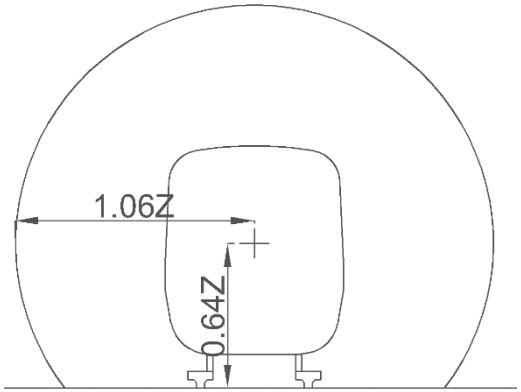

T1. *L/Z*=147. *α*=0%.

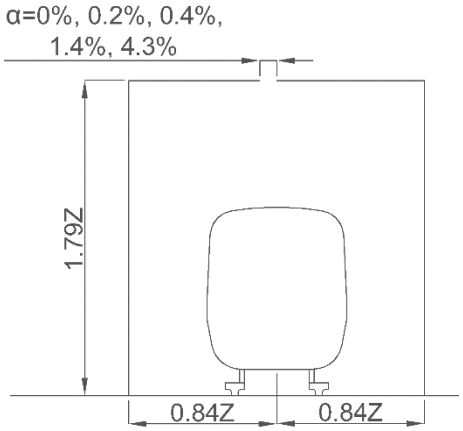

T2. *L/Z*=51. *α*=0%, 0.4%.

T3. *L/Z*=13. *α*= 0%, 0.2%, 0.4%, 1.4%, 4.3%.

T4. *L/Z*=5. *α*=0%.

Figure 4. Cross-section views and descriptions of the structures.

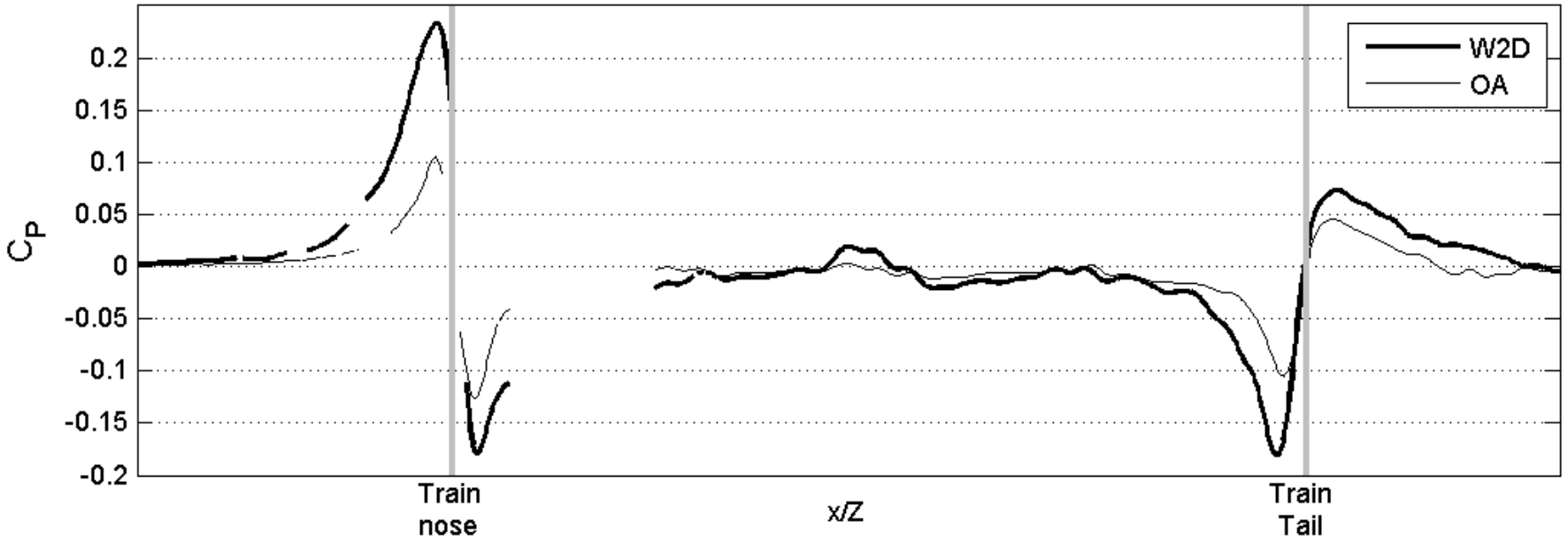

Figure 5. Time history of the pressure field around the train, in the open air and symmetrical double wall case W2D. An in-flow probe was located at x_P/Z=31, y/Z=0.65, z/Z=0.58.

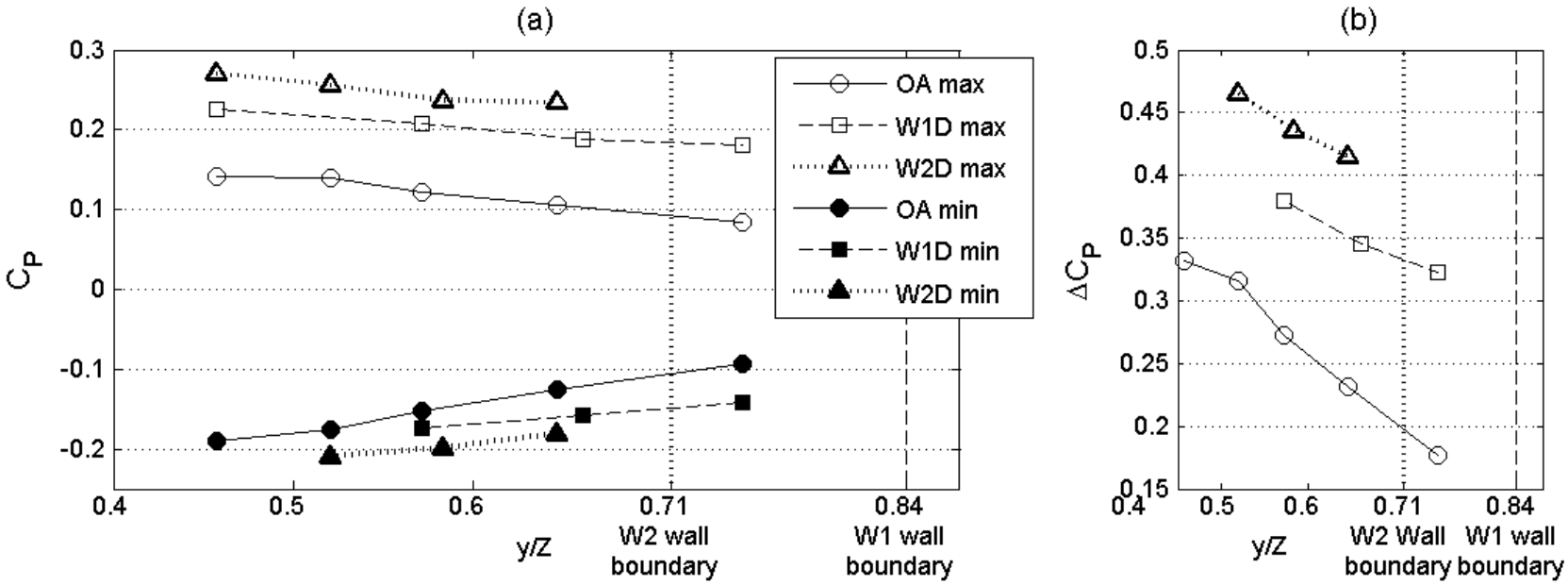

Figure 6. Open air and double wall cases. Variation of in-flow pressure along the *y*-axis, at height *z*/*Z*=0.58. (a) Maximum and minimum pressure; (b) Peak-to-peak pressure change.

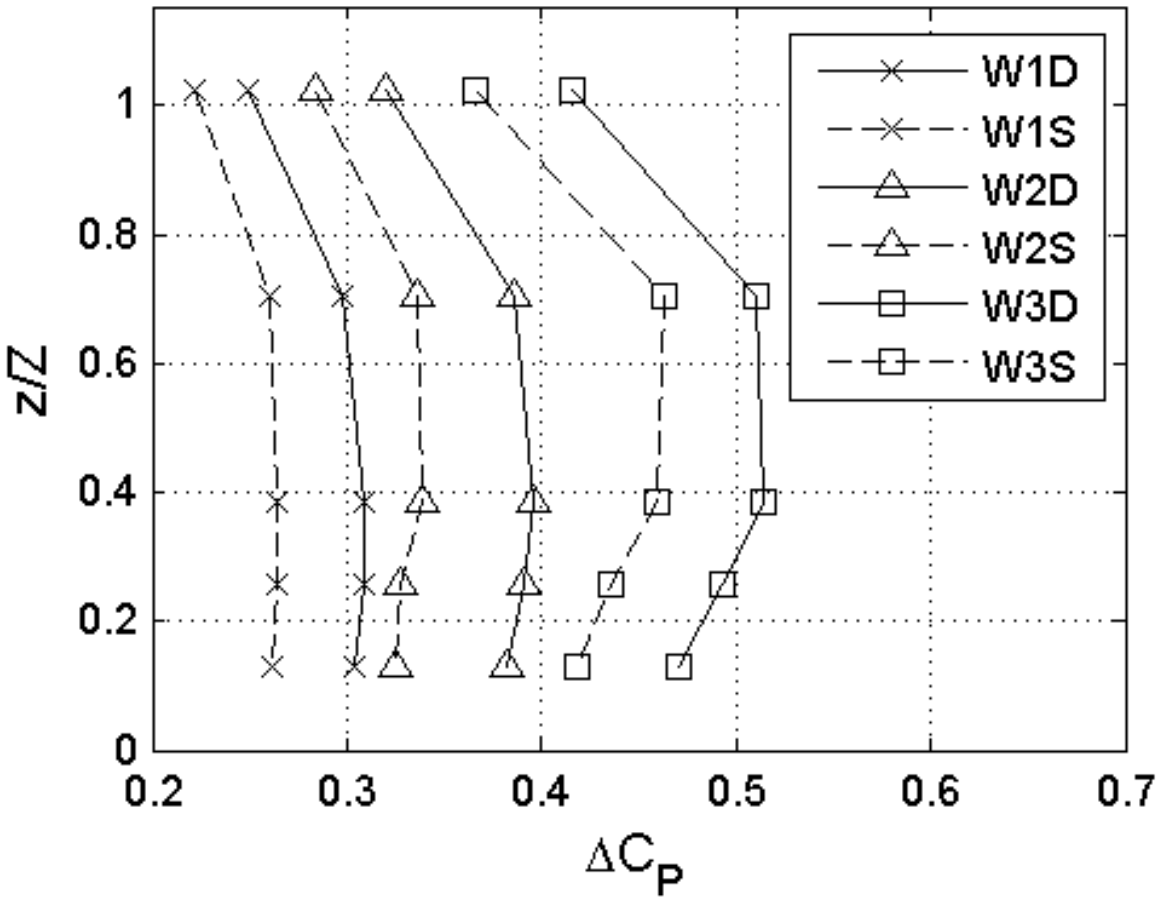

Figure 7. Wall cases. Variation of the peak-to-peak surface pressure change along the *z*-axis, for single and double wall cases.

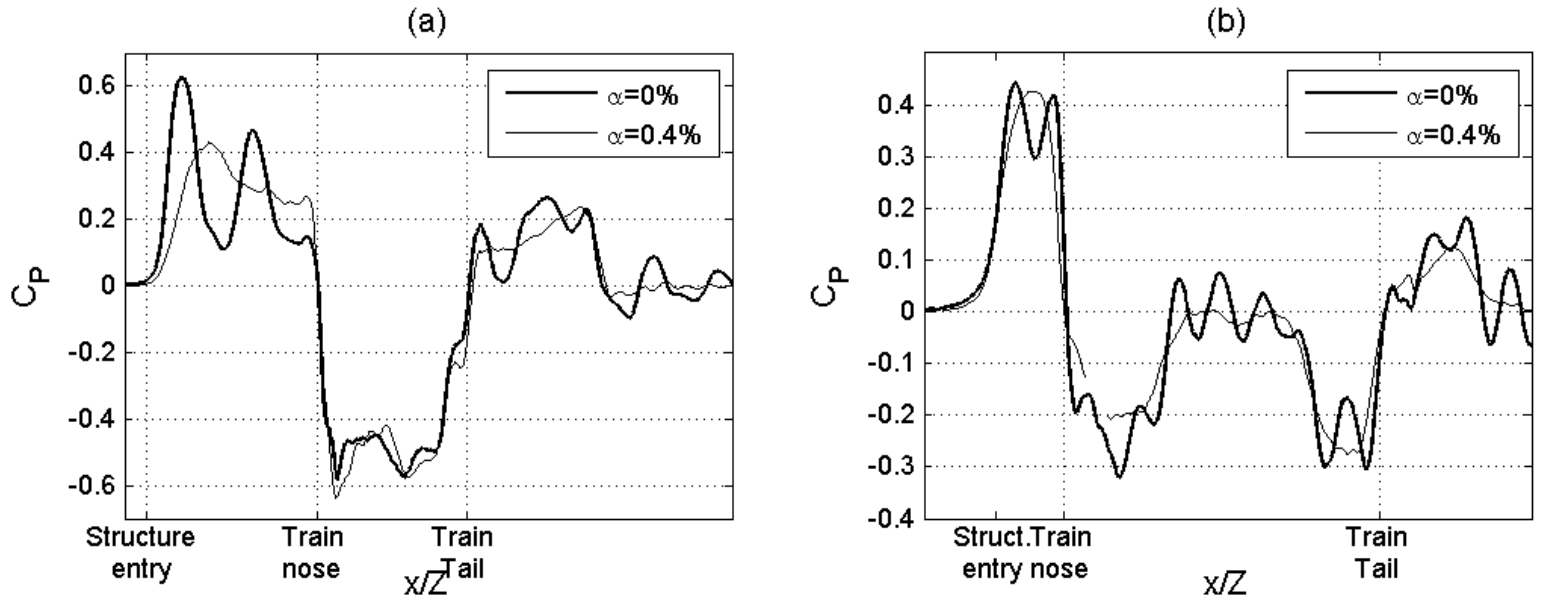

Figure 8. Short tunnels. The effect of pressure waves; The pressure in a sealed tunnel, measured by a surface tapping, is compared with the pressure in an unsealed tunnel which allows the pressure waves to dissipate quickly. The tapping location is z/Z=0.26. Tunnels: (a) T2, where L/Z=51 and x_P/L=62%; (b) T3, where L/Z=13 and x_P/L=45%.

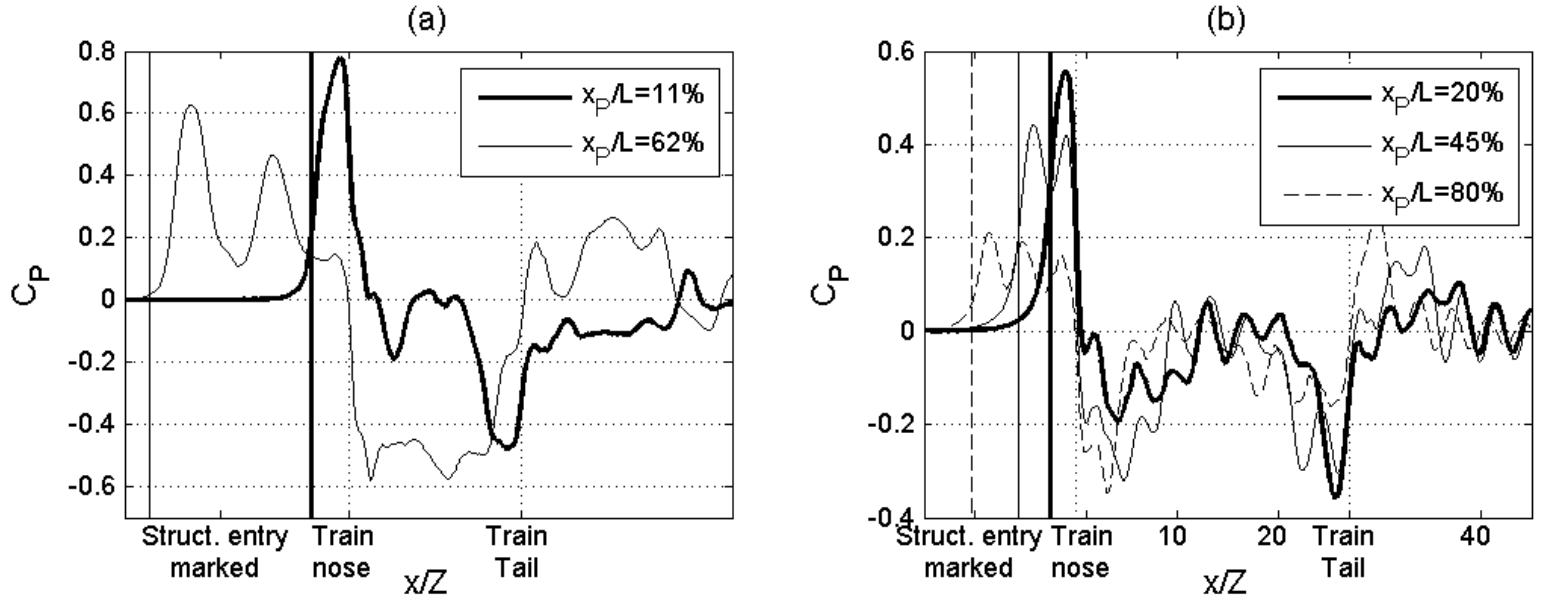

Figure 9. Short tunnels. The pressure measured at various locations within the tunnels, expressed as dimensionless percentages (x_P/L). The surface tapping height is z/Z=0.26. The tunnels are sealed (α=0%). Vertical lines represent the train nose entering the tunnel. Tunnels: (a) T2; (b) T3.

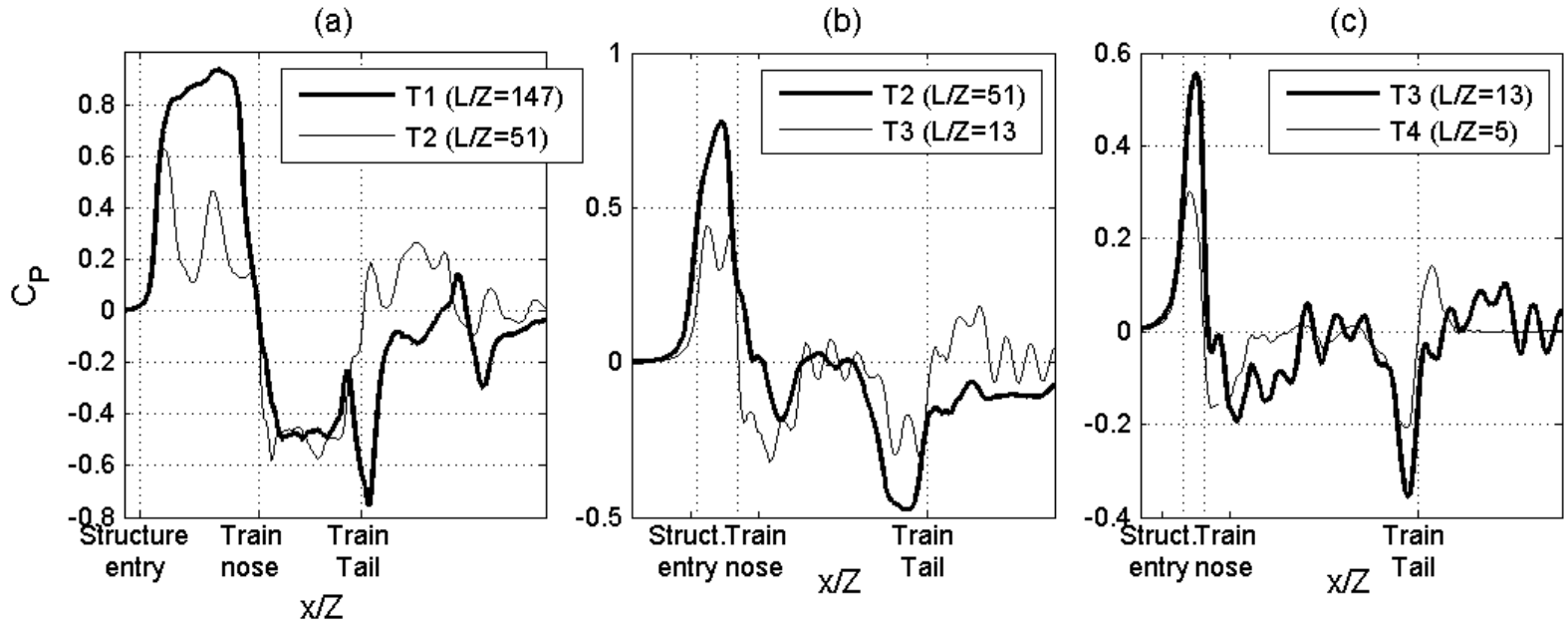

Figure 10. Short tunnels. The pressure measured for tunnels of different lengths, when the surface tapping is at a constant distance from the entrance. The tunnels are sealed (α=0%). The tapping height is z/Z=0.26, and the distance of the tapping from entrance in each plot is: (a) x_P/Z=31; (b) x_P/Z=6; (c) x_P/Z=2.6.

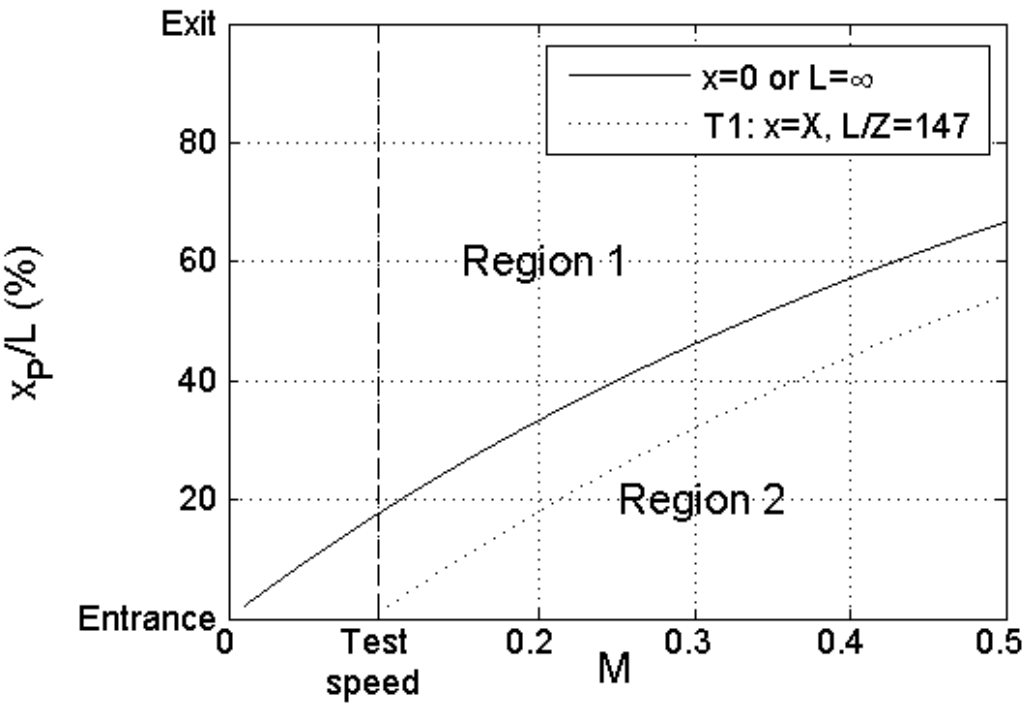

Figure 11. Tunnels. Visualization showing how far into a tunnel an observer may detect the same results at a given point relative to the train nose (x) regardless of tunnel length (L). Two values of x and L are plotted.

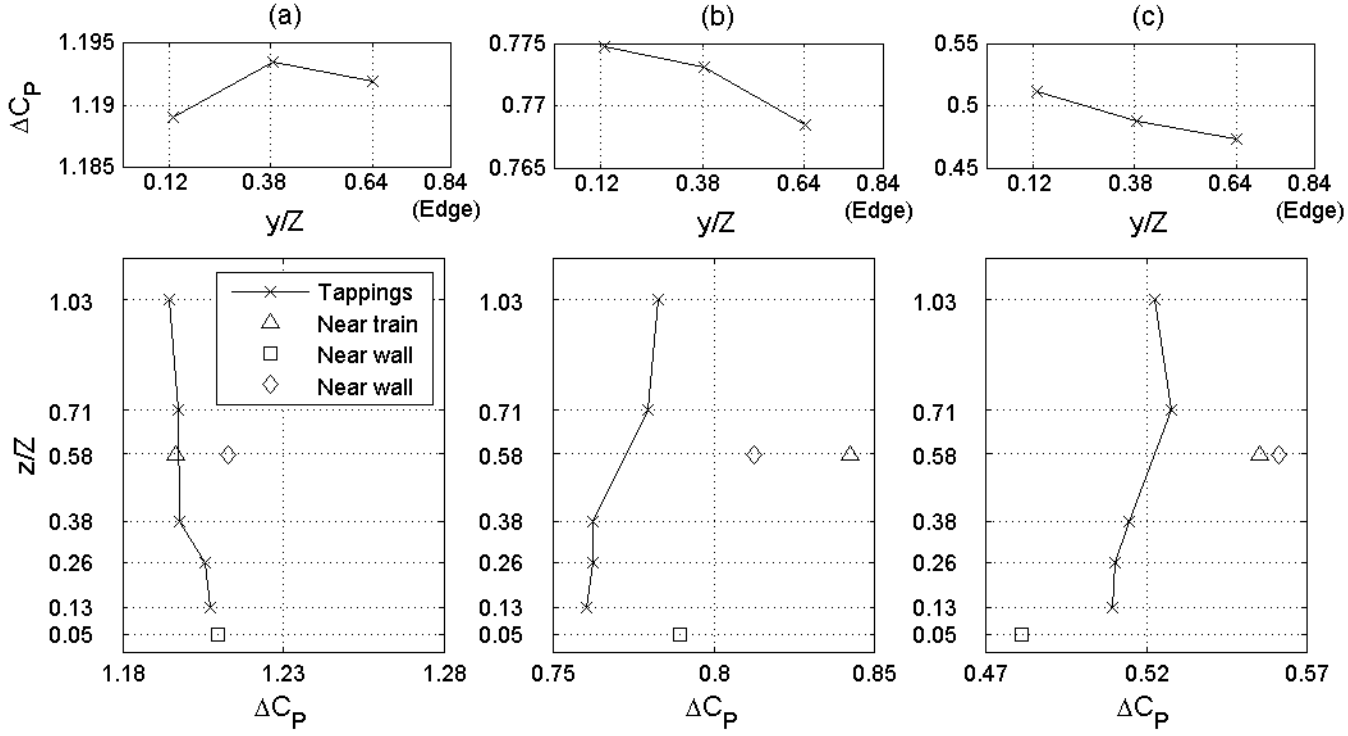

Figure 12. Short tunnels. Variation of the peak to peak pressure change for the wall and ceiling tappings, and in-flow probes, for tunnels: (a) T2, where L/Z=51 and x_P/L=62%; (b) T3, where L/Z=13 and x_P/L=45%; (c) T4, where L/Z=5 and x_P/L=50%.

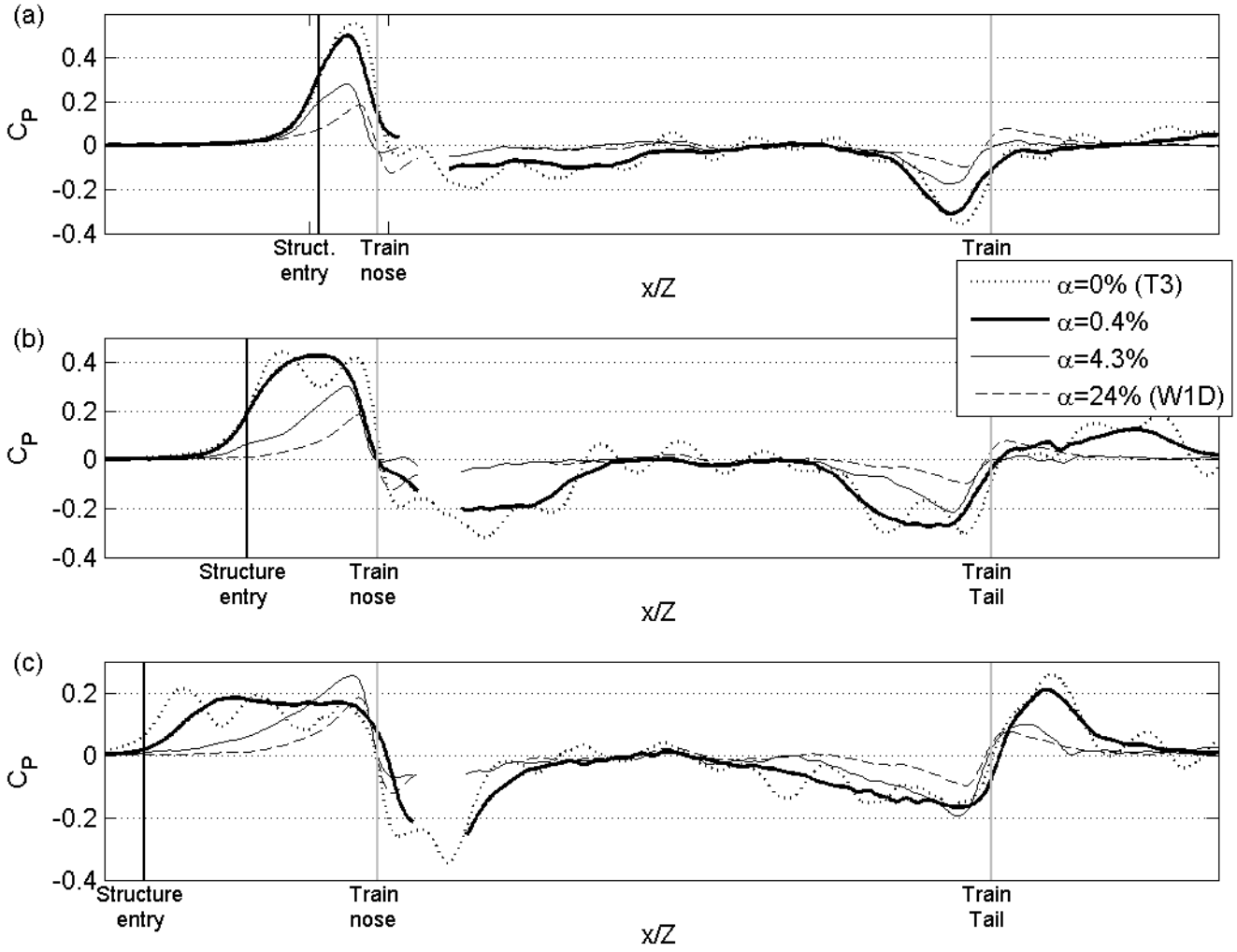

Figure 13. Partially-enclosed spaces (L/Z=13). Pressure measured for four α values at three x-positions within the structures. The tapping height is z/Z=0.26. Locations: (a) x_P/L=20%; (b) x_P/L=45%; (c) x_P/L=80%.

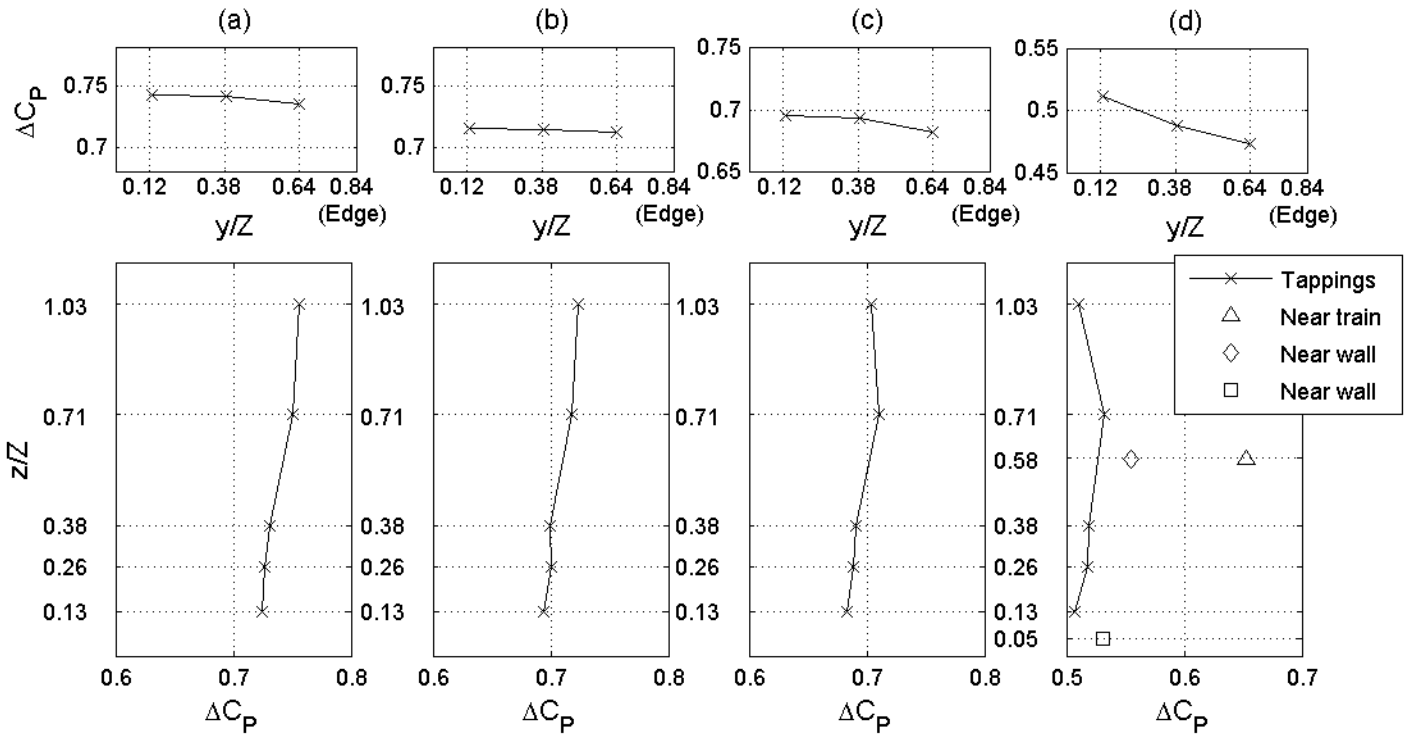

Figure 14. Partially-enclosed spaces (L/Z=13). Variation of the peak to peak pressure change for the wall and ceiling tappings, and in-flow probes, for α values: (a) α=0.2%; (b) α=0.4%; (c) α=1.4%; (d) α=4.3%.